Brazilian Journal of Physics
ISSN: 0103-9733
luizno.bjp@gmail.com
Sociedade Brasileira de Física
Brasil

Colnaghi Fernandes, Jessica; Mulato, Marcelo
Effective Area Effects on the Final Device Sensitivity of Ion Sensor Transducers
Brazilian Journal of Physics, vol. 45, núm. 4, agosto, 2015, pp. 387-393
Sociedade Brasileira de Física
São Paulo, Brasil

Braz J Phys (2015) 45:387–393
DOI 10.1007/s13538-015-0328-9

SOCIEDADE BRASILEIRA DE FÍSICA

CONDENSED MATTER

Effective Area Effects on the Final Device Sensitivity of Ion Sensor Transducers

Jessica Colnaghi Fernandes[1] · **Marcelo Mulato**[1]

Received: 29 January 2015 / Published online: 9 May 2015

Abstract Fluorine-doped tin oxide (SnO_2:F) was used as the ion-sensing layer of an EGFET-pH sensor. The effective area affects the final results, as well as the sensor surface potential and sensitivity. The sensor miniaturization is highly required on medical applications, with that the effective area must be properly understood. Routine insertion and removal of total and partial surface areas in buffer solution were analyzed and compared. The results show that the routine changes considerable the sensor sensitivity. Variations in the double layer, Helmholtz plane, and Gouy-Chapman region play a significant role. The final sensitivities of the samples were compared with values available in the literature, even for other materials. The role that area normalization plays in quality assessment is discussed for proper future technological miniaturizations.

Keywords EGFET · pH sensor · Area normalized sensitivity

1 Introduction

Researchers have developed ion sensitive field effect transistors (ISFETs) on the basis of the metal oxide field effect transistor (MOSFET) [1]. Bergveld fabricated the first ISFET, a device with wide application as pH sensor [2]. ISFET devices have proven to be promising tools in various research domains, including DNA genotyping, food screening, and multi-analyte detection for biomedical applications [3] and [4]. Many chemical and biological processes depend on one of the commonest laboratory measurements—the pH value [5] and [6]. ISFETs are based on ion attachment on a film surface. Variation in the surface potential modifies the electric field in the insulator-semiconductor FET interface. Hence, the ions concentration in solution modulates the electric current intensity through the MOSFET. The ISFET technology allows the use of microfabrication processes, which enables miniaturization. The fact that ISFETs are small, respond rapidly, and are compatible with conventional integrated circuits makes them an excellent choice for biosensor applications [7]. However, it is not possible to change the ion-sensitive film in an ISFET device. An alternative to ISFETs is to use the extended gate field effect transistor (EGFET). The EGFET structure isolates the FET from the chemical environment, which is not feasible in an ISFET device. The EGFET is separated into two parts: the first is the sensitive part; the second is the commercial MOSFET. As a pH sensor, the EGFET can help to detect and quantify any kind of substances that can produce or consume protons, like an enzyme, which makes it widely applicable as biosensor [8].

Several materials have been tested as the ion-sensing element of EGFET [9–14]. The electrical and optical properties of fluorine-doped tin oxide (SnO_2:F) films have been investigated in the past [15]. Tin oxide is a multifaceted material that has been used for numerous applications [16], including optoelectronic devices, as well as electrodes in various types of solar cells [17] and in gas-sensing or gas monitoring devices [18]. In a previous study, we had already discussed the temporal evolution, the influence of light, and the sensor response as a function of the operating temperature of the solution where the sample is immersed [19]. The present

✉ Jessica Colnaghi Fernandes
jessicacf@pg.ffclrp.usp.br

[1] Universidade de São Paulo, Av. Bandeirantes, 3900 Ribeirão Preto, SP, Brazil

paper investigates how the effective immersed area of the dipped sample impacts the sensor response using SnO_2:F as the EGFET sensitive element. Given the fact that different literature data correspond to a large range of sensing materials and procedures, then a detailed investigation about effective areas and dipping procedures justify this study. In this sense, as discussed later in this paper, not only the obtained sensitivities but also the temporal evolution and the eventual miniaturization of devices to be used as biosensors should be carefully examined.

2 Experiments

The commercial samples were obtained from Flexitec Company. The SnO_2:F films presented a sheet resistance of 23 Ω/sqr. The starting films were cut into four pieces of different areas, which were designated as T-samples, as detailed in Table 1. The electric contacts in all the samples were made using a thin copper wire and conductive silver paint. An epoxy resin was employed to encapsulate the electric contact.

A silver reference electrode was connected to the drain of a commercial MOSFET (CD4007, Texas Instruments), and the SnO_2:F sample was connected to its gate, to give the EGFET device. The source terminal of the MOSFET was grounded. Both the silver reference electrode and the sensing structure were dipped into the buffer solution, purchased from CINETICA and with pH in the range 2–12. Figure 1a shows the structure of the EGFET device, where V_{ref} is the reference voltage, V_{ds} is the voltage between the drain (D) and the source (S), and V_{gs} is the voltage between the gate (G) and the source, given by $V_{ref} + \Delta V$. In this case, ΔV is the potential difference between the solution and the surface of the sensing film.

The drain-source current, I_{ds}, was measured using an HP Data Acquisition 34970A apparatus. An Agilent E3646A Dual Output DC Power Supply was also employed. Figure 1b displays the typical $I_{ds\ x}\ V_{ds}$ (solid line) and I_{ds} x V_{ref} (dashed line) experimental curves. The $I_{ds\ x}\ V_{ds}$ data were obtained by varying the drain-source voltage while keeping the gate-source voltage constant at 5 V. In the other configuration, the I_{ds} x V_{ref} data were acquired by varying the gate-source voltage while the drain-source voltage was kept constant at 5 V. For the first set of experiments called total area (T), four individual samples with different effective total areas ranging from 42 to 230 mm^2 were used. In this case, the samples were labeled T1 to T4, from the smallest to the largest area (see Table 1).

Two other different routines were also performed. Figure 1c depicts a detailed scheme of the part of the SnO_2:F

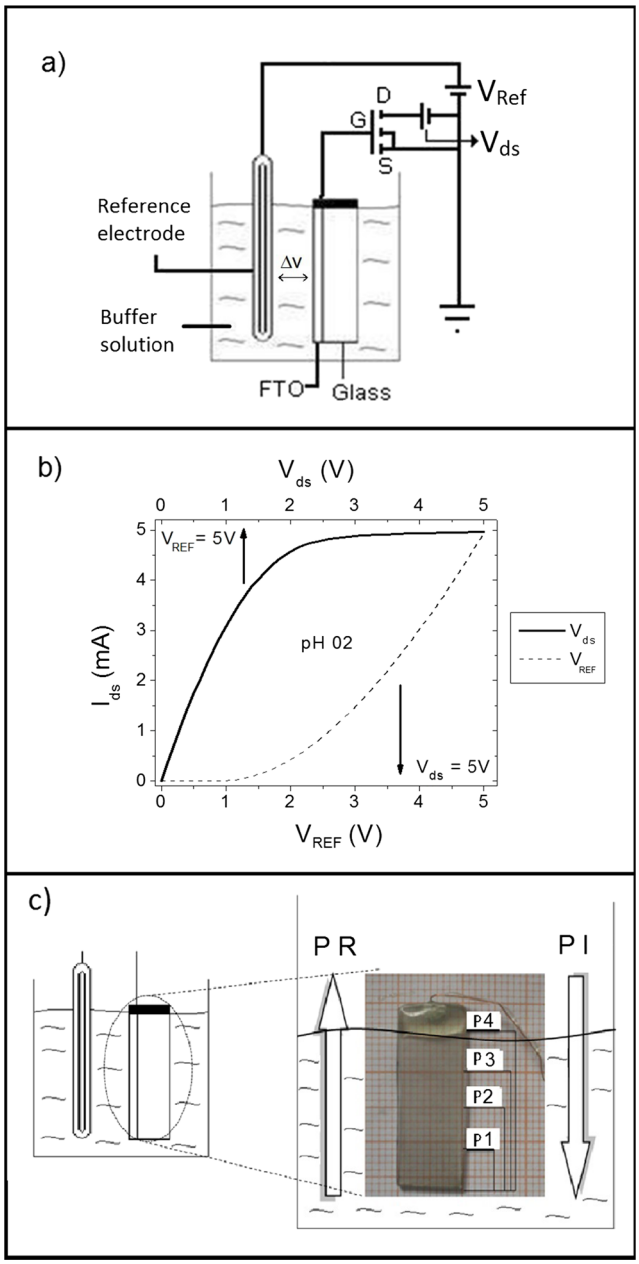

Fig. 1 **a** Structure of EGFET measurement system, where $V_{gs} = V_{ref} + \Delta V$; **b** Typical $I_{ds\ x}\ V_{ds}$ (*solid line*) and $I_{ds\ x}\ V_{ref}$ (*dashed line*) curves for pH = 2; and **c** Measurement sequence scheme: *PR* and *PI* represent partial removal and partial insertion of the sample, respectively

Table 1 Samples description according to the effective areas of the SnO_2:F samples with sheet resistance of 23 Ω/sqr

Sample	Area (mm^2)	Sample	Area (mm^2)
T1	42	P1	60
T2	100	P2	120
T3	170	P3	170
T4	230	P4	230

T stands for total area; *P* stands for partial area

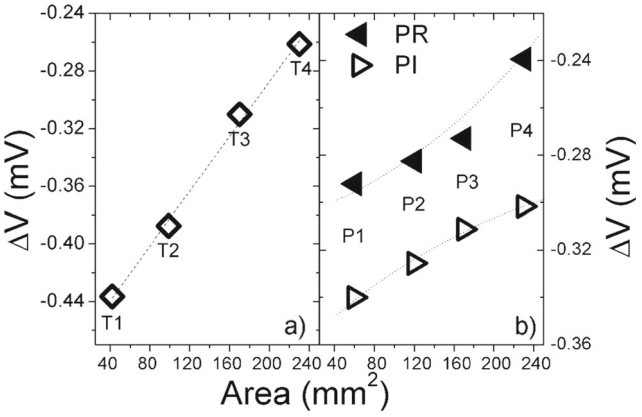

Fig. 2 ΔV as a function of the sample area for SnO_2:F samples using the V_{ds} configuration. **a** Total area measurements and **b** partial area measurements: PI for insertion routine and PR for removal routine

sample that was dipped into the desired buffer solution (using the designated P samples in Table 1). In the first routine, designated partially inserting sequence (PI) hereafter, a sample was inserted in the buffer solution with different exposed areas. The immersed areas were 60, 120, 170, and 230 mm^2. In the second routine, designated partially removing sequence (PR), the whole sample was inserted into the buffer solution, and then small parts were sequentially removed. All the samples were washed with Milli-DI water for 15 min before each new run, and a stabilization time of 10 s was allowed before each measurement. All measurements were performed in the dark, at room temperature.

3 Results and Discussion

The I_{ds} x V_{ds} curves for the two measurement configurations described previously was construct, for a fixed pH equal to 2. Thus, the I_{ds} values were recorded for the largest V_{ds} bias. From experimental I_{ds} data, corresponding ΔV values was calculated and plotted in Fig. 2. Figure 2a corresponds to values for the T-samples completely immersed in the buffer solution. A linear behavior is observed.

The starting sample is n-doped by fabrication. The application of a V_{ref} potential to the electrode immersed in the solution in which the sample resides increases the amount of positive charges near the surface of the film (Fig. 3). The Helmholtz plane (HP) will arise between the SnO_2:F surface electrons and the solution ions [20]. A region of diffused charges extends from the Helmholtz plane interface to the bulk of the solution, called the Gouy-Chapman region [20]. Starting from a place in the solution that is far away from the sample, the electric potential increases until the end of the Gouy-Chapman region (right to left in Fig. 3), followed by a decrease along the Helmholtz plane. Electrons accumulated close to the film surface create an internal electric field variation with a new positive slope (Fig. 3).

The net potential variation, as described by the previously discussed ΔV, numerically originates from the sum of these components. So, the V_{gs} value has to be lower than the applied V_{ref} potential, to lead to a negative ΔV, as shown in Fig. 2.

Consider the case of a specific buffer solution where the reference electrode sits at a fixed potential. Ion accumulation at the surface of the sensing film likely presents fixed density distribution. If a simple capacitance effect takes place, the potential difference inside the film will remain constant regardless of the used area. The same might happen to the potential inside the Helmholtz plane. However, as a consequence of reduced film area, the Gouy-Chapman region will also reduce, leading to a smaller value of the electrical potential. The final Vgs potential for a smaller sensing film will also be smaller. According to the schematic drawing in Fig. 3, this could lead to final ΔV with larger modulus. Figure 2a reveals that this is indeed the case. Note that for a total area variation with a factor of about 5, ΔV varies by a factor of about 2. This suggests that a non-linear variation of the spatial charge distribution happens together with changes in total area.

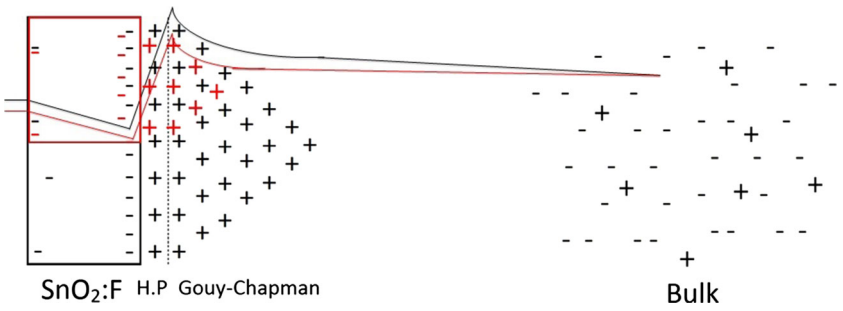

Fig. 3 Qualitative scheme for the Helmholtz plane (HP) and Gouy-Chapman region for samples with different surface areas. Larger surface area (*black lines*) produces a higher amount of positive charges in Gouy-Chapman region, while smaller areas produces a smaller amount of the positive charges in the region (*red lines*). The electrical potential changes proportional to the amount of charges in Gouy-Chapman region

Figure 2b contains ΔV values for the so-called partial area (P) samples. Solid symbols represent the results achieved during the PR measurements and evidence that ΔV displays the same qualitative behavior as in Fig. 2a. For PR, the first measurement occurs with total immersion of the sample (P4), followed by the smaller areas (P3, P2, and P1) upon sample removal from the buffer solution. During the first measurement, most of the free binding sites of the sample surface participate in the formation of the double-layer region. Smaller surface area decreases the Gouy-Chapman region, leading to a larger final ΔV modulus. The non-linear behavior stems from the fact that the part of the sample removed from the solution still contains some surface charges, which contributes to less pronounced ΔV reduction, as expected from the discussion about Fig. 2a.

For PI, represented by the open symbols in Fig. 2b, the first measurement involves the smallest area P1. The second measurement uses a larger area (P2) and adds a new surface region containing extra free binding sites that had not been in contact with the solution yet. The length of the Gouy-Chapman region increases and produces a smaller potential variation along its length, leading to a smaller final ΔV modulus. The same behavior occurs for P3 and P4. Note that in this case, there is no memory effect, so the response is even more linear than in the case of the previously discussed PR. Hence, the measurement sequence plays a fundamental role on the final results.

The sensitivities also change when the used surface area varies (Fig. 4). For all the measurements, the sensitivity diminishes with decreasing area, but for PR and PI, these changes are smaller than for T. The sensitivities are different even when the area is the same (for different P and T samples in Fig. 4). Considering the largest area in Fig. 4, the specific comparison of the results for samples T4 and P4 shows that quality dispersion exists inside the same starting batch. Additionally, comparison of the results obtained for sample P4 using two different routines reinforces that memory effects matter.

Figure 5 illustrates the final ΔV as a function of the nominal area for the V_{ds} (left) and V_{gs} (right) curves, for buffer solutions with different pH—acid (pH 2), neutral (pH 7), and alkaline (pH 12)—using the P samples. The solid circles correspond to the PR sequence, whereas the empty squares refer to the PI sequence. Similar qualitative behaviors can be observed for both measurements at each pH. For all the tested pHs, the absolute ΔV value is larger for V_{gs} than for V_{ds} experiments. For the V_{ds} measurements, the varying voltage is applied between the drain and the source of the MOSFET. The MOSFET device does not into contact with the electrolyte solution (due to the use of the extended gate), so the drain-source voltage is unaffected by the ions of the electrolyte solution. On the other hand, for Vgs measurements, the externally biased voltage is applied between the source and the reference electrode sitting inside the solution. This happens in individually controlled steps, and no measurement takes place during voltage variation. The surface potential at the SnO_2:F film depends on the final ionic distribution and adsorption and determines the state of the gate electrode. Therefore, the ions distribution dynamics in the solution determines the final MOSFET current, and variations in ΔV reflect this.

Figure 5a, b show that the absolute ΔV value increases with decreasing area, as already discussed in Fig. 3 for the case presented in Fig. 2b.

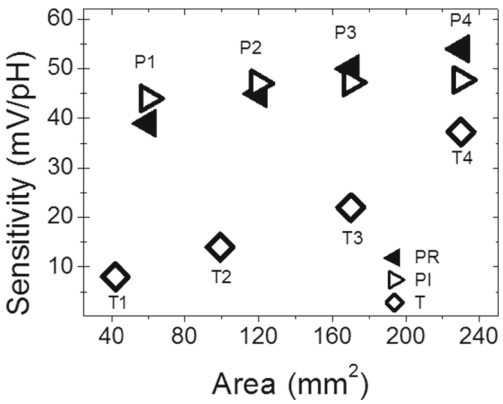

Fig. 4 Sensitivity as a function of the surface area for the three different experiments: total area (T), partial insertion (PI), and partial removal (PR)

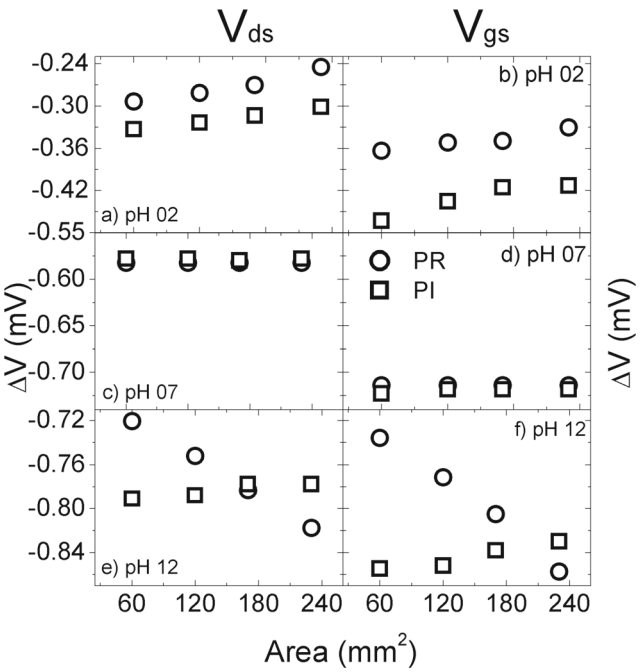

Fig. 5 Final ΔV as a function of sample area for both Vds (*left*) and Vgs (*right*) system configurations for buffer solutions with different pH: pH 2 in (**a**) and (**b**), pH 7 in (**c**) and (**d**), and pH 12 in (**e**) and (**f**)

No variation occurs as a function of the area or sequence of measurement for pH 7. So, the system sits close to the isoelectric point of the sensing film as previously stated in reference [19]. Important differences between V_{ds} and V_{gs} configurations are only observable in Fig. 5c, d, agreeing with the previous discussion about electric field variation inside the buffer solution for the V_{gs} set-up. As expected, larger absolute ΔV values emerge in this case. At pH 12, interesting results arise (Fig. 5e, f). For the PI, everything happens as previously discussed for area variation and measurement configuration, while for PR the opposite occurs.

The main reason behind this fact seems to be the slower ionic dynamic at higher pH. In the case of PI, the area increases when the first part is not saturated yet. Ions keep joining the surface of both the former and the recently inserted part and the absolute ΔV value decreases. Concerning PR, immersion of the total area does not saturate the surface. Partial sample removal should lead to larger ΔV absolute value. Nevertheless, the part of the sample that remains immersed in the solution keeps receiving ions close to the surface because the dynamics is slower. So, the ΔV absolute value falls due to the slow ion dynamics added to the surface reduction. Hence, the measurement sequence

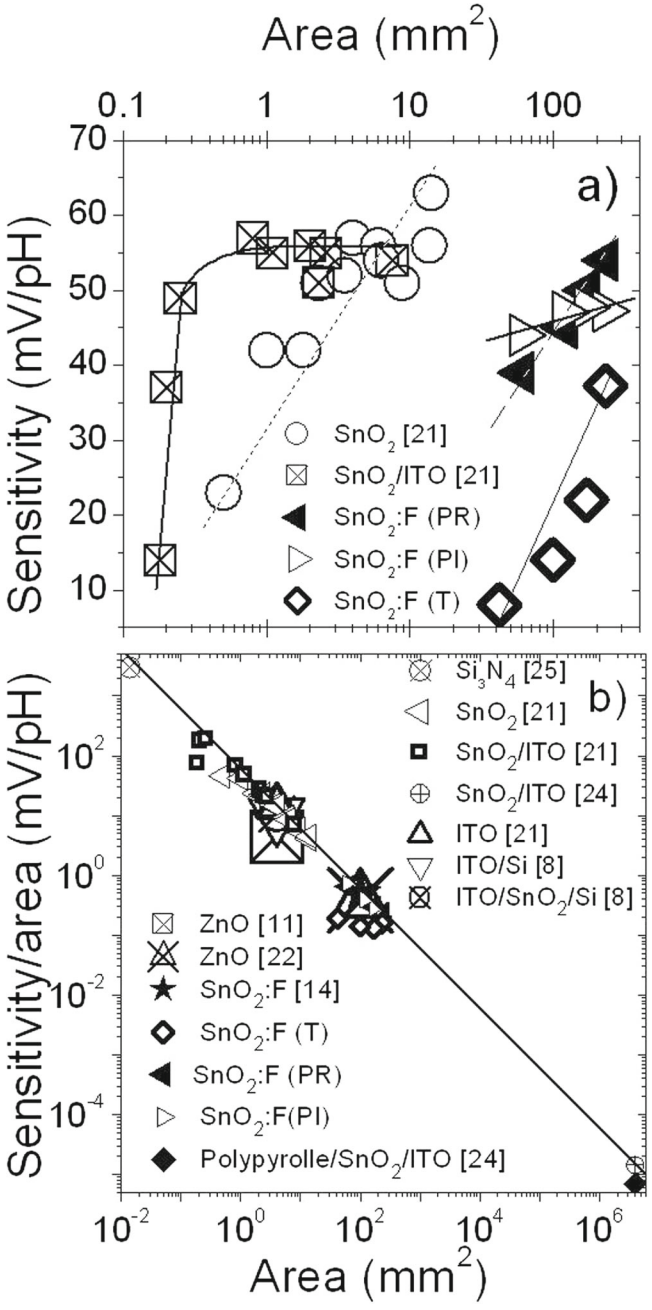

Fig. 6 **a** Sensitivity as a function of sample area for different tin oxide samples. *Solid and dashed lines* are guides for the eyes only. **b** Area normalized sensitivity as a function of sample area for several materials. The *solid line* corresponds to the Nernst prediction

is important indeed. Also, it is essential to take care when developing sensors based on microfluids. It is crucial to avoid transient effects, to account for memory effect, and to use the recommended set-up configuration with stationary states.

An essential parameter to characterize a sensor is its sensitivity. The literature brings various values for different materials and effective areas. A comparative study that leads to a final standardization is necessary. Figure 6a presents the sensitivity of several tin oxide samples used as sensitive EGFET layer as a function of the sensors area. The present data are compared with the literature [21]. The lines are just a guide for the eyes. The sensitivity usually diminishes with decreasing area, indicating that poorer quality materials might stem from scale reduction. Data in literature are commonly related only to sensitivity without taking area account. Numerical variations up to a factor 6 may arise for the same material grown under the same nominal conditions and so the impact on miniaturized sensors would be enormous.

A proposal for standardization would be to use a parameter described by the sensitivity divided by the sensors effective area. Figure 6b shows the sensitivity/area (S/A) for several materials used as sensitive layer for pH sensors. The figure includes data from the present contribution as well as literature results for ZnO [11] and [22], ITO/Si [23], ITO /SnO_2 /Si [23], SnO_2 /ITO [21] and [24], polypyrrole / SnO_2 / ITO [24], Si_3N_4 [25], ITO [21], and SnO_2:F [14] and [21]. The solid line represents the theoretical Nernst sensitivity for potentiometric sensors, which is equal to 59.2 mV/pH [26]. According to the data in Fig. 6b, Si_3N_4 (in the top-left part of the figure) seems to be the best material for use in miniaturized sensors: besides presenting the smallest area, it still remains with an S/A value close to the maximum value predicted by Nernst. Figure 7a, b were construct by zooming specific regions of Fig. 6b in order to help to better visualize the two piled subgroups close to areas 1 and 100 mm^2, respectively.

Since the S/A line represent the expected optimized values, sub deviations suggest a reduced quality of the final materials. According to the present analysis, any material can potentially achieve the optimized S/A relation; e.g, final values that lie on the expected S/A line. However, when miniaturization is an issue, the final result should be close to the up-left region of the S/A theoretical curve. This has been the first time this kind of analysis and standardization has appeared in the literature, so we believe the present work shall contribute to better comparison among different materials and sensors in the future.

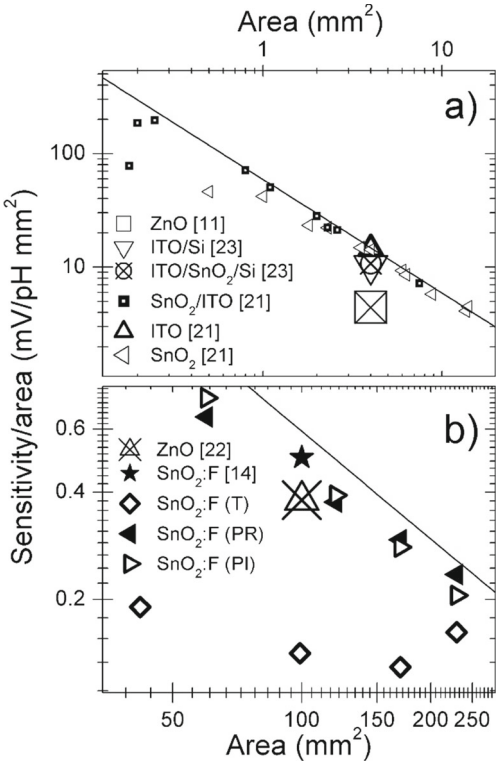

Fig. 7 Zoomed specific regions from Fig. 6b corresponding to two piled subgroups according to the area range: **a** below 10 mm^2 and **b** from 10 to 100 mm^2

4 Conclusions

The surface potential of the sensing part of an EGFET varies linearly as a function of surface area. Smaller immersed areas lead to higher final ΔV absolute value due to the smaller Gouy-Chapman region. The sequence routine can play a significant role. When the surface area decreases through process that removes the sample from the buffer solution, memory effects cause ions to remain on the non-immersed part of the samples. A smaller than expected surface potential variation occurs, culminating in a non-linear function, which might be important during micro fluidic systems design and application. V_{ds} measurements do not alter the ion dynamics inside the buffer solution, in contrast to V_{gs} measurements. The net balance of slow ion dynamics and surface reduction leads the ΔV absolute value to decrease unexpectedly in alkaline pH. Comparison of sensors quality using only the sensitivity as gold parameter might be misleading. The use of varied literature data shows that area-normalized sensitivity is better even to compare a wide range of sensing materials which is crucial when miniaturizing optimized sensors.

Acknowledgments The authors thanks Prof. I. Hummelgen for providing the samples and M.Sc. R. A. S. Nascimento for experimental help. This study was supported by FAPESP, CAPES, and CNPq Brazilian funding agencies.

References

1. J.-C. Lin, B.-R. Huang, Y.-K. Yang, IGZO nanoparticle-modified silicon nanowires as extended-gate field-effect transistor pH sensors. Sensors Actuators B Chem. **184**, 27–32 (2013)
2. H.-H. Li, C.-E. Yang, C.-C. Kei, C.-Y. Su, W.-S. Dai, J.-K. Tseng, P.-Y. Yang, J.-C. Chou, H.-C. Cheng, Coaxial-structured ZnO/silicon nanowires extended-gate field-effect transistor as pH sensor. Thin Solid Films **529**, 173–176 (2013)
3. P. Bergveld, Development of an ion-sensitive solid-state device for neurophysiological measurements. IEEE Trans. Biomed. Eng. BME **17**(1), 7071 (1970)
4. D. Braeken, D.R. Rand, A. Andrei, R. Huys, M.E. Spira, S. Yitzchaik, J. Shappir, G. Borghs, G. Callewaert, C. Bartic, Glutamate sensing with enzyme-modified floating-gate field effect transistors. Biosens. Bioelectron. **24**(8), 2384–2389 (2009)
5. P.D. Batista, M. Mulato, C.F.D.O. Graeff, F.J.R. Fernandez, F.D.C. Marques, SnO_2 extended gate field-effect transistor as pH sensor. Braz. J. Phys. **136**(2 A), 478–481 (2006)
6. C.-Y. Chen, H.-L. Hsieh, C.-H. Lin, S.-K. Liao, T.-P. Sun, C.T.-S. Ching, P.-L. Liu, Extended gate H^+-ion sensitive field effect transistor with signal interface. in *Proceedings of the 2009 2nd International Conference on Biomedical Engineering and Informatics, BMEI 2009*, (2009)
7. H.-J. Jang, J.-G. Gu, W.-J. Cho, Sensitivity enhancement of amorphous InGaZnO thin film transistor based extended gate field-effect transistors with dual-gate operation. Sensors Actuators B Chem. **181**, 880–884 (2013)
8. M. Turek, M. Keusgen, A. Poghossian, A. Mulchandani, J. Wang, M.J. Schning, Enzyme-modified electrolyte-insulator-semiconductor sensors. J. Contemp. Phys. Armen. Acad. Sci. **43**(2), 82–85 (2008)
9. E.S. Ferreira, M. Mulato, Thallium bromide deposited using spray coating. Braz. J. Phys. **42**(34), 186–191 (2012)
10. E.J. Guidelli, E.M. Guerra, M. Mulato, Vanadium and titanium mixed oxide films: synthesis, characterization and application as ion sensor. J. Electrochem. Soc. **159**(6), J217–J222 (2012)
11. P.D. Batista, M. Mulato, ZnO extended-gate field-effect transistors as pH sensors. Appl. Phys. Lett. **87**(14), 1–3 (2005)
12. E.M. Guerra, G.R. Silva, M. Mulato, Extended gate field effect transistor using V_2O_5 xerogel sensing membrane by sol-gel method. Solid State Sci. **11**(2), 456–460 (2009)
13. J.C. Ugucioni, T. Ghilardi Netto, M. Mulato, Mercuric iodide composite films using polyamide, polycarbonate and polystyrene fabricated by casting. Nucl. Instruments Methods Phys. Res. Sect. Accel. Spectrometers Detect. Assoc. Equip. **622**(1), 157–163 (2010)
14. P.D. Batista, M. Mulato, Polycrystalline fluorine-doped tin oxide as sensoring thin film in EGFET pH sensor. J. Mater. Sci. **45**(20), 5478–5481 (2010)
15. T. Minaai, A. Nara, M. Kumagai, S. Tanemura, M. Tanemura, Adsorption and desorption properties on the fluorine-doped tin oxide film surface on a glass substrate under UV light irradiation in vacuum. Vacuum **80**(9), 957–961 (2006)
16. A.V. Moholkar, S.M. Pawar, K.Y. Rajpure, P.S. Patil, C.H. Bhosale, Properties of highly oriented spray-deposited fluorine-doped tin oxide thin films on glass substrates of different thickness. J. Phys. Chem. Solids **68**(10), 1981–1988 (2007)
17. M.G. Helander, M.T. Greiner, Z.B. Wang, W.M. Tang, Z.H. Lu, Work function of fluorine doped tin oxide. J. Vac. Sci. Technol. **29**(1), 11–19 (2011)
18. M.C. Carotta, M.A. Butturi, G. Martinelli, D. Vona, M.L.S. Licoccia, E. Traversa, Thick film microsensors based on nanosized titania sol–gel powder. Electron Technol. **33**(1-2), 113–117 (2000)
19. J.C. Fernandes, M. Mulato, *Charge sensing properties of nanostructured fluorine-doped tin oxide surfaces* (presented at the ECS 223, Toronto, Ontario, Canada, 2013)
20. D.E. Yates, S. Levine, T.W. Healy, Site-binding model of the electrical double layer at the oxide/water interface. J. Chem. Soc. Faraday Trans. 1 Phys. Chem. Condens. Phases **70**(0), 1807–1818 (1974)
21. L.-T. Yin, J.-C. Chou, W.-Y. Chung, T.-P. Sun, S.-K. Hsiung, Separate structure extended gate H^+-ion sensitive field effect transistor on a glass substrate. Sensors Actuators B Chem. **71**(12), 106–111 (2000)
22. J.-L. Chiang, J.-F. Hsu, S.-F. Lee, L.-Y. Lee, H.-Y. Liu, Ion sensitivity of the flowerlike ZnO nanorods synthesized by the hydrothermal process. J. Vac. Sci. Technol. B **27**(3), 1462–1465 (2009)
23. J.-L. Chiang, S.-S. Jhan, S.-C. Hsieh, A.-L. Huang, Hydrogen ion sensors based on indium tin oxide thin film using radio frequency sputtering system. Thin Solid Films **517**(17), 4805–4809 (2009)
24. C.-W. Pan, J.-C. Chou, I.-K. Kao, T.-P. Sun, S.-K. Hsiung, Using polypyrrole as the contrast pH detector to fabricate a whole solid-state pH sensing device. IEEE Sensors J. **3**(2), 164–170 (2003)
25. Y. Kagohashi, H. Ozawa, S. Uno, K. Nakazato, K. Ohdaira, H. Matsumura, Complementary metal-oxide-semiconductor ion-sensitive field-effect transistor sensor array with silicon nitride film formed by catalytic chemical vapor deposition as an ion-sensitive membrane. Jpn. J. Appl. Phys. **149**(1), Part 2 (2010)
26. S. Levine, A.L. Smith, Theory of the differential capacity of the oxide/aqueous electrolyte interface. Discuss. Faraday Soc. **52**(0), 290–301 (1971)